Research Square

Preprints are preliminary reports that have not undergone peer review.
They should not be considered conclusive, used to inform clinical practice,
or referenced by the media as validated information.

The second extracellular loop gates Stachel-mediated activation of ADGRG6/GPR126

Patrick Scheerer

patrick.scheerer@charite.de

Charité - Universitätsmedizin Berlin https://orcid.org/0000-0001-5028-2075

Franziska Wiechert

Charité - Universitätsmedizin Berlin, Institute of Medical Physics and Biophysics

Michal Szczepek

Charité

Gunnar Kleinau

Institute of Medical Physics and Biophysics, Charité - Universitätsmedizin https://orcid.org/0000-0003-2131-671X

Lisa Kupsch

Leipzig University, Rudolf Schönheimer Institute of Biochemistry

Amal Hassan Ali

Charité - Universitätsmedizin Berlin, Institute of Medical Physics and Biophysics, Group Protein X-ray Crystallography and Signal Transduction

Monique Gallandi

Charité - Universitätsmedizin Berlin, Institute of Medical Physics and Biophysics, Group Protein X-ray Crystallography and Signal Transduction

Andrea Schmidt

Charité - Universitätsmedizin Berlin, Institute of Medical Physics and Biophysics, Group Protein X-ray Crystallography and Signal Transduction

David Speck

Charité - Universitätsmedizin Berlin, Institute of Medical Physics and Biophysics, Group Protein X-ray Crystallography and Signal Transduction

Anja Koch

Charité - Universitätsmedizin Berlin, Institute of Medical Physics and Biophysics, Group Protein X-ray Crystallography and Signal Transduction

Justus Loerke

Charité - Universitätsmedizin Berlin, Institute of Medical Physics and Biophysics
https://orcid.org/0000-0002-3424-8536

Thiemo Sprink

Charité - Universitätsmedizin Berlin, Core Facility for cryo-Electron Microscopy / Max Delbrück Center for Moleculare Medicin in the Helmholtz Association (MDC), Technology Plat https://orcid.org/0000-0002-0760-6828

Tarek Hilal

Freie Universität Berlin, Research Center of Electron Microscopy and Core Facility BioSupraMol https://orcid.org/0000-0002-7833-8058

Christian Spahn

Charite – Berlin University of Medicine https://orcid.org/0000-0002-2939-9487

Torsten Schöneberg

Leipzig University, Rudolf Schönheimer Institute of Biochemistry https://orcid.org/0000-0001-5313-0237

Ines Liebscher

Leipzig University, Rudolf Schönheimer Institute of Biochemistry https://orcid.org/0000-0003-4480-8987

Article

Keywords: G protein-coupled receptor, adhesion GPCR, second extracellular loop, GPR126, ADGRG6, structure determination, CTF structure

Posted Date: October 26th, 2026

DOI: https://doi.org/10.21203/rs.3.rs-11087611/v1

License: This work is licensed under a Creative Commons Attribution 4.0 International License. Read Full License

Additional Declarations: There is **NO** Competing Interest.

Abstract

Over the past decade, numerous studies have shown for several adhesion GPCRs (aGPCRs) that signaling activity is regulated by an intramolecular agonist (termed *Stachel*) with a conserved amino acid core located proximal to the N terminus of transmembrane helix 1. Here we present cryo-EM structures of the human ADGRG6 (or GPR126) C-terminal fragment bound to heterotrimeric Gs protein in two distinct conformational states — an "ECL2-in" state that sterically and allosterically limits *Stachel* engagement and a "*Stachel*-bound" active state with a core orientation unknown so far — determined to global resolutions of 3.4 Å and 3.8 Å, respectively. In the "ECL2-in" state the central segment of this loop makes a network of hydrogen-bonding and van-der-Waals contacts with the transmembrane domain. Of note, the conserved TM3–ECL2 cysteines do not form the canonical disulfide bridge in the "ECL2-in" conformation. Structure-guided mutagenesis, peptide stimulation and cellular signaling assays map inactivating and constitutively activating variants to spatially distinct ECL2 regions.

Together, these data establish ECL2 as an intramolecular, tunable gate that controls internal-agonist engagement and G-protein activation in GPR126, revealing a structural mechanism that can be exploited to bias aGPCR signaling and might support new ideas for rational ligand design.

INTRODUCTION

The class B family of G protein–coupled receptors (GPCRs) comprises secretin-like receptors (class B1) and adhesion GPCRs (aGPCRs; class B2). The aGPCR family includes 33 members in humans that can be subdivided into several groups [1–3] (Fig. 1a). These receptors regulate diverse physiological processes, including cell proliferation and intercellular communication, and play key roles in sensing and transducing mechanical forces during cell–cell and cell–matrix interactions [4–7]. Consequently, dysregulation of aGPCR signaling contributes to a wide range of pathological conditions, including cancer [8,9].

Like other GPCRs, aGPCRs share a conserved architecture consisting of an extracellular N terminus (Nt), a seven-transmembrane helix domain (7TMD), and a cytosolic C terminus (Ct). A defining feature of most aGPCRs is their extended Nt containing multiple extracellular domains, including a GPCR autoproteolysis-inducing (GAIN) domain. The GAIN domain harbors a GPCR Proteolysis Site (GPS) characterized by an autocleavable HXS/T motif [10,11] that mediates autoproteolytic cleavage, generating an N-terminal fragment (NTF) and a C-terminal fragment (CTF). In many aGPCRs, the N-terminal region of the CTF immediately adjacent to the GPS contains a short peptide sequence termed the *Stachel* [12]. This sequence consists of a conserved *Stachel* core of eight residues and a variable linker connecting the core to transmembrane helix (TMH) 1 [5,13,14]. Functional studies, including *Stachel*-core mutagenesis and activation by synthetic *Stachel*-derived peptides support the idea that the *Stachel* acts as an intramolecular agonist of the receptor [14].

Structural models propose that in the inactive state the *Stachel* core adopts a β-strand conformation buried within the GAIN domain (the “in-GAIN” state), whereas isolated *Stachel* peptides are largely unfolded [15]. Upon receptor activation, the *Stachel* is thought to be released from the GAIN domain and to insert into the extracellular vestibule of the 7TMD, where it adopts a short helical conformation. However, the structural basis of this transition and the molecular determinants that regulate *Stachel* engagement with the 7TMD remain poorly understood.

Recent structural studies have begun to provide insights into aGPCR activation through the determination of several CTF structures [13,16] (Extended Data Table 1), particularly for members of the ADGRG group (Fig. 1a). For GPR126 (also known as ADGRG6), available structures include a zebrafish NTF (PDB-ID: 6V55 [17]) and a recently reported apomorphine-bound human GPR126-CTF–G_s complex (PDB-ID: 21DU [18]), which displays features of *Stachel* binding similar to those observed in other aGPCR structures. GPR126 plays essential roles in peripheral nervous system myelination and regulates osteoblast and adipocyte differentiation[19,20]. The receptor responds to diverse extracellular cues, including mechanical forces [21] and binding to laminin-211 [4] or collagen IV/VI [22,23]. Despite these advances, the mechanisms that control *Stachel* engagement with the 7TMD and the structural intermediates involved in receptor activation remain largely unresolved.

Here we report two cryogenic electron microscopy (cryo-EM) structures of the human GPR126 C-terminal fragment (GPR126-CTF) that reveal unexpected features of receptor activation. In one structure, extracellular loop 2 (ECL2) is inserted into the 7TMD and occupies much of the canonical *Stachel*-binding pocket (variant designated $GPR126_{ECL2–in}$). Although the *Stachel* sequence itself is not resolved, the receptor is captured in complex with a G protein, indicating an intracellularly active conformation. A second structure, determined at lower resolution, reveals a distinct *Stachel*-core–bound conformation that differs from previously reported aGPCR CTF structures [24–28] and may represent an intermediate state during receptor activation.

Complementary mutagenesis and signaling analyses of both the CTF and full-length GPR126 (GPR126-FL) demonstrate that multiple ECL2 residues are critical for regulating basal receptor activity as well as *Stachel* peptide–induced signaling and activation by mechanical stimuli. Together, these findings identify ECL2 as a key intramolecular regulator of aGPCR activation. More broadly, our results reveal an unexpected regulatory role of extracellular loop architecture in controlling *Stachel*-mediated signaling, thereby expanding current models of adhesion GPCR activation and suggesting new mechanistic parallels with regulatory principles established for class A GPCRs [29–36].

RESULTS

To determine the structure of the human GPR126-CTF, we generated a construct comprising amino acid residues 854–1250, which includes the *Stachel* sequence. Enhanced green fluorescent protein (eGFP) was fused to the C terminus to enhance protein expression (Extended Data Fig. 1). The heterotrimeric

dominant-negative G_sαβγ protein was co-expressed with the CTF in insect cells to facilitate in-cell complex formation (Extended Data Fig. 2). To stabilize the complex during purification, nanobody 35 (Nb35) was added following cell lysis. After detergent solubilization, affinity purification, and size-exclusion chromatography, the GPR126-CTF–G_s protein–Nb35 complex was concentrated and vitrified for cryo-EM analysis (Extended Data Fig. 3).

Two active-state-like GPR126-CTF–G_s complexes reveal distinct ECL2 and Stachel features

Cryo-EM reconstructions of GPR126-CTF revealed complexes with heterotrimeric G_s and Nb35 (Fig. 1b). Particle classification separated two major 7TMD conformations (Extended Data Fig. 4). Population *i* (75%, 101,791 particles): GPR126 with ECL2 partially occupying the canonical *Stachel*-binding site, hereafter $GPR126_{ECL2-in}$ (Fig. 1c–d). The *Stachel* sequence was not visible in the 7TMD. Cryo-EM maps at 3.27 Å global resolution (local resolution up to 2.4 Å) allowed modeling of most side chains (Extended Data Fig. 4).

Population *ii* (25%, 33,792 particles): GPR126 with the *Stachel* core bound in the 7TMD, termed $GPR126_{Stachel-in}$, albeit in a fold distinct from previously reported CTF–*Stachel* structures [13,18]. Resolved at 3.76 Å, the maps confirmed *Stachel* engagement but, due to limited local resolution (> 4 Å), side chain positions could not be assigned. This conformation likely represents an alternative or intermediate binding state (Fig. 2a–b).

Backbone comparison of $GPR126_{ECL2-in}$, $GPR126_{Stachel-in}$, and the published GPR126-CTF–*Stachel* structure (PDB-ID: 21DU [18]) revealed pronounced differences in TMH7 and ECL3 positioning. In the *Stachel*-unbound $GPR126_{ECL2-in}$ structure, ECL3 lies close to ECL2, together covering the extracellular *Stachel*-binding pocket (Fig. 2c). In *Stachel*-bound states, TMH7 directly interacts with the *Stachel* core and ECL3 adopts an outward orientation (Fig. 2d). Notably, the intracellular arrangement of G_s is nearly identical in both complexes (Extended Data Fig. 5).

Although the *Stachel* is absent in $GPR126_{ECL2-in}$, the receptor adopts an active-like conformation, as evidenced by G-protein engagement. ECL2 is fully resolved (Extended Data Fig. 6), a feature previously reported only for GPR114 (PDB-ID: 7EQ1 [5]) and GPR97 (PDB-ID: 7d76 [26]). Unlike these receptors, GPR126 ECL2 is deeply inserted into the crevice formed by TMH extracellular ends and ECL1–ECL3 (Fig. 1c). In both $GPR126_{Stachel-in}$ and the published CTF–*Stachel* structures, ECL2 is partially unresolved, spanning residues G972–E983 (this study) or S975–G981 (PDB-ID: 21DU). Interestingly, ECL2 is extended in most human group VIII aGPCRs, though sequence conservation is limited to a few N- and C-terminal residues (Fig. 1e).

Absence of the canonical disulfide bridge between conserved cysteines in TMH3 (C3.33) and ECL2 (C45.50) in $GPR126_{ECL2-in}$

A striking feature of the $GPR126_{ECL2-in}$ structure, compared to both *Stachel*-bound CTF structures (own CTF *Stachel*-in and PDB-ID: 21DU [18]), is the absence of the canonical disulfide bridge between the conserved cysteines in TMH3 ($C^{3.33}$) and ECL2 ($C^{45.50}$; numbering according to the unified class B ECL2 system [13]). In our cryo-EM map, the distance between the cysteine side chains is ~ 3.7 Å, which is too long to support a covalent disulfide bond (Extended Data Figs. 7 and 9). While this disulfide is clearly resolved in some aGPCR structures, such as GPR133 (PDB-ID: 7WU2 [37]), inspection of ~ 10 available aGPCR CTF cryo-EM maps (Extended Data Table 1) show that in several cases the cysteine pairs are similarly too distant for covalent linkage, and density corresponding to a disulfide bond is absent. In these instances, automated model building may have incorporated the disulfide bridge based on the assumption of conservation. Notably, a recent vasopressin type 1a receptor structure also lacking this typically conserved disulfide bridge was reported (PDB-ID: 9XB1 [38]).

Distinct ECL2 amino acid substitutions in the GPR126-CTF modulate basal activity and peptide p126-mediated signaling

We next analyzed conserved ECL2 residues and their interactions with the 7TMD in the $CTF_{ECL2-in}$ structure (Extended Data Figs. 8–9). Several amino acid side chains in TMH3, TMH5 and ECL3 lie within contact distance of ECL2 residues (Extended Data Fig. 9c). Of particular interest are the conserved ECL2 residues Y971 ($Y^{45.36}$), W986 ($W^{45.51}$) and I987 ($I^{45.52}$) (Fig. 1e). Notably, in the $GPR126_{ECL2-in}$ structure the side chains of Y971 and W986 deviate from the conserved orientations observed in other aGPCR-CTF structures (Extended Data Fig. 9a), with W986 displaying an approximately 90° rotation. By contrast, the conserved $W^{6.55}$ in TMH6 adopts the same orientation as in the GPR126 $CTF_{Stachel-in}$ structure (Extended Data Fig. 9a) and in other aGPCRs. In addition, tight interactions exist between ECL2 and several TMD residues located in spatially distinct regions, including TMH1, TMH3 and TMH5. Together, these observations suggest that alterations in ECL2 conformation or amino-acid composition could affect receptor function, pointing to a regulatory role of ECL2 in GPR126 signaling.

To test the proposed functional contributions of individual ECL2 residues, we generated mutations within the ECL2 of the human GPR126-CTF (underlined sequence: 964-SRNNNEVYGKESYGKEKGDEFCWIQD-989) (Fig. 3a). Residues were selected based on high evolutionary conservation, altered side chain orientation relative to other aGPCR structures, or proximity to the canonical *Stachel*-core binding site (Fig. 2c). Because the otherwise conserved disulfide bridge between TMH3 (C902) and ECL2 (C985) was not observed in the $CTF_{ECL2-in}$ structure, these cysteine residues were also substituted. In addition, we generated an ECL2 deletion variant (GPR126-CTF ΔECL2; deletion of residues 974-ESYGKEKG-981) lacking the central loop region (Fig. 3a). To specifically examine the role of ECL2 in *Stachel*-mediated signaling, we further generated constructs lacking the *Stachel* sequence (CTF ΔStachel; deletion of residues 813-THFGVLMDLPRS-824), containing an inactivated *Stachel* core (CTF M819A), or combining these alterations with ECL2 mutations (CTF ΔStachelΔECL2, CTF ΔStachel Y976A, CTF ΔStachel

D982A). All constructs were analyzed for total and cell-surface expression as well as signaling activity using cAMP assays (Extended Data Table 2).

Overall, total cellular expression of most mutants was comparable to that of the wild-type receptor (WT), whereas cell-surface expression varied substantially between constructs (Extended Data Table 2). ECL2 mutants Y976A, D982A and ΔECL2 exhibited elevated basal cAMP levels, indicating constitutive activity (constitutively active mutants, CAMs) (Fig. 3b, c), despite reduced surface expression. In contrast, mutants within the *Stachel* sequence displayed reduced basal activity (Fig. 3d) while showing normal or even increased expression levels. Reducing transfected plasmid amounts to normalize surface expression (Extended Data Table 2) did not proportionally alter signaling responses. Notably, single substitutions E974A, Y976A and D982A displayed constitutive activity (Fig. 3c) and spatially cluster near the previously described p126 binding site (Extended Data Fig. 10).

Mutations affecting central ECL2 residues (E974A and K978A), as well as deletion of the loop core (ΔECL2), permitted WT-like or even enhanced activation by the agonistic peptide p126 (Fig. 3c). By contrast, substitutions C902S (TMH3) and C985S (ECL2), or mutation of conserved residues within ECL2 (Y971A, F984A, W986A), abolished p126-mediated activation. These inactivating variants cluster at the interface between ECL2 and TMH2/TMH3 (Extended Data Fig. 10).

Together, these findings indicate that specific alterations within ECL2 modulate both basal activity and ligand-induced signaling of the GPR126-CTF, suggesting that this loop contributes to the regulation of receptor activity. The increased p126-mediated stimulation observed for the ECL2-core deletion and the E974A/K978A variants (Fig. 3c) further supports the conclusion that the WT ECL2 partially restrains *Stachel*-mediated activation, likely through competition with the *Stachel* core as suggested by the GPR126-CTF$_{ECL2-in}$ structure (Fig. 2c). Consistent with this interpretation, the elevated basal activity of the ECL2 mutants Y976A and D982A, both located near the putative *Stachel*-core binding site, was abolished when combined with *Stachel* deletion, recapitulating the effect of *Stachel* inactivation alone (ΔStachel, M819A) (Fig. 3d). In contrast, peptide-induced activation remained intact, demonstrating that the loss of activity in ECL2/*Stachel* mutants is *Stachel*-dependent. These findings indicate that ECL2 does not function as an intramolecular agonist (built-in agonist) but instead limits activation by the endogenous *Stachel* core. Constitutive activation observed for mutants Y976A, D982A and ΔECL2 likely reflects an increased accessibility or binding capacity of the endogenous *Stachel* peptide, resulting from reduced steric hindrance caused by shorter alanine side chains or by shortening of the ECL2 loop.

The ECL2 in full-length GPR126 contributes to activity regulation but differs functionally from the GPR126-CTF ECL2

We next examined whether ECL2 also regulates activity of the full-length receptor, to assess similarities and differences between the naturally occurring full-length and cleaved receptor forms. Consistent with the corresponding GPR126-CTF mutants, deletion of the ECL2 core (GPR126-FL ΔECL2) and several single substitutions within the ECL2 core region (K973A, E974A, K978A, and E979A) increased basal activity (Fig. 3e). Notably, none of the FL or CTF ECL2 mutants reduced basal signaling, further indicating

that ECL2 itself does not mediate receptor activation (Fig. 3c, e). Moreover, peptides of different lengths derived from the ECL2 sequence did not affect basal or p126-induced activity of either FL or CTF receptors (Extended Data Fig. 11a–d).

Similar to the GPR126-CTF mutant K978A, which showed enhanced peptide responsiveness, the corresponding GPR126-FL variant was higher activated by p126 than WT. However, several mutations produced distinct functional effects in FL versus CTF receptors. Whereas the GPR126-CTF mutant E974A responded to p126 similarly to WT, the GPR126-FL E974A variant lost peptide responsiveness. In addition, p126 induced higher cAMP levels in GPR126-FL Y976A than in wild-type GPR126-FL (Fig. 3e), while stimulation of the corresponding GPR126-CTF mutant remained unchanged relative to WT (although it displayed constitutive activity). Most strikingly, the cysteine mutants C902S and C985S had no effect on basal or p126-mediated activation in the GPR126-FL receptor (Fig. 3e), in contrast to the complete loss of activity observed in the corresponding GPR126-CTF mutants (Fig. 3c).

GPR126-FL can also be activated by N-terminal antibody binding [39] or by mechanical stimulation (shaking) [7]. Deletion of the ECL2 core, as well as substitutions Y971A, F984A, W986A and the cysteine mutants C902S and C985S, significantly enhanced antibody-induced activation (Fig. 3f). These residues are highly conserved at the N- and C-terminal ends of ECL2. Notably, the same mutations abolished p126-mediated signaling in the GPR126-CTF (Fig. 3c) but not in the GPR126-FL. In contrast, strong mechanical stimulation by shaking produced higher overall activation levels but did not reveal differences between mutants and WT GPR126 (Extended Data Fig. 11e), suggesting that the magnitude or type of external stimulus influences the role of ECL2 in receptor activity regulation.

DISCUSSION

The ECL2 as a “gatekeeper” of the Stachel agonist – multistep intramolecular regulation in GPR126

In this study cryo-EM maps of GPR126 reveal two distinct conformational populations. In the predominant class (75% of particles), ECL2 is deeply threaded into the helical bundle (Fig. 1c–d), partially occupying the space normally filled by the *Stachel* sequence in other aGPCR structures, including the recently reported GPR126-CTF (PDB-ID: 21DU [18]) and other ADGRG group VIII receptors, such as GPR114/ADGRG5 and GPR97/ADGRG3 (Extended Data Table 1). In these structures, the *Stachel* core is inserted into a TMD pocket, and ECL2 does not occupy the site [13]. The only other available “apo” aGPCR TMD structure is GPR64/ADGRG2 (PDB-ID: 7YP7 [25]), in which ECL2 likewise does not occupy the *Stachel* binding site. In our $GPR126_{ECL2\text{-}in}$ structure, the *Stachel* is not resolved, suggesting it has been displaced. Importantly, our data do not resolve the sequence of events preceding complex formation; for example, the *Stachel* core may have initially activated the receptor and then been displaced by ECL2 (and ECL3). Regardless, the $GPR126_{ECL2\text{-}in}$ structure represents a novel “active-like” state in which the *Stachel* is displaced by the ECL2.

The minor particle population (25%) yielded a structure with an inserted *Stachel* ($GPR126_{Stachel\text{-}in}$) at slightly lower resolution (3.8 Å). The *Stachel* core adopts a fold and binding mode distinct from the recently determined GPR126-CTF structure [18] (Fig. 2), indicating that *Stachel* binding should be flexible. Together, these two conformations suggest a potential dynamic equilibrium: under some conditions (perhaps in our overexpression system) ECL2 preferentially occupies the TMD pocket, yet the receptor can still adopt a classical *Stachel*-bound active conformation.

Because the intracellular G_s protein is bound in the GPR126-$CTF_{ECL2\text{-}in}$ state, ECL2 may stabilize an active-like receptor conformation. Analogous "self-agonist" roles of ECL2 have been observed in several class A GPCRs. In GPR17, ECL2 inserts into the ligand-binding site to promote constitutive activation [40], and in the orphan GPR21/GPR52 family, an agonist-like motif in ECL2 drives high basal activity [35,41]. Viral GPCRs similarly exploit ECL2: EBV BILF1 caps the ligand pocket for constitutive signaling [42], and KSHV GPCR's apo-structure shows ECL2 folded into the pocket to sustain basal G-protein coupling [43].

However, our functional assays indicate that in GPR126, ECL2 restrains *Stachel*-mediated signaling. In the CTF, which mimics the cleaved, *Stachel*-exposed state, mutations or deletion of central ECL2 residues (Y976A, D982A, ΔECL2) markedly increase basal cAMP levels (Fig. 3b–c). These constitutively active mutants likely relieve ECL2-mediated blockade of the *Stachel* binding pocket, allowing the *Stachel* core to engage. Conversely, mutations of ECL2 (Y971A, F984A, W986A) or cysteine substitutions (C902S, C985S) abolish p126 activation (Fig. 3c–d). These inactivating variants cluster at the interface between ECL2 and TMH2/3 near the conserved Y971–W986 pair (Extended data Fig. 10), likely disrupting receptor folding or proper ECL2 positioning and preventing *Stachel* binding. Importantly, combining activating ECL2 mutations (Y976A, D982A) with *Stachel* deletion or inactivation (ΔStachel, M819A) abolishes elevated basal signaling (Fig. 3e), indicating that the increased activity of these mutants is entirely *Stachel*-dependent. Together, these data support a "gatekeeping" model: intact ECL2 sterically hinders *Stachel* engagement, keeping basal activity low, while displacement or mutation of ECL2 permits the *Stachel* to access the TMD with increasing signaling. Analogous mechanisms are seen in other GPCRs, such as LGR7/RXFP1, where ECL2 movement is required for activation [34].

Distinct conserved residues in the N- and C-terminal ECL2 regulate mechanosensitivity

Adhesion GPCRs are well-known mechanosensors, and our data indicate that ECL2 contributes to force responses. Activation of full-length GPR126-FL by an N-terminal HA-tag (mimicking ligand engagement) is enhanced in ECL2 mutants that disrupt *Stachel* gating (ΔECL2, Y971A, F984A, W986A) (Fig. 3f). These residues localize at the base or flanks of ECL2, implying that their alteration lowers the energetic barrier for ECL2 displacement under force. In contrast, vigorous shaking produced no differential effect, suggesting that only specific force regimes (e.g., shear stress or pulling) exploit the ECL2 "latch." Extracellular forces or ligand binding may therefore induce ECL2 displacement, unleashing the *Stachel* agonist. Similar ECL2-dependent mechanosensitivity has been proposed in class A GPR68 [44,45]. These

findings again support a model in which ECL2 functions as a gate: in its resting position it restrains activation, whereas under tension it moves to permit signaling.

Mechanistic model and implications

These results suggest a multistep model for GPR126 activation. In the resting GPR126-FL receptor, the *Stachel* is likely trapped in the GAIN domain, while ECL2 occupies a TMD pocket (as in the GPR126-$CTF_{ECL2\text{-}in}$ structure). Physiological stimulation, such as mechanical force or NTF-binding ligands, modulates the GAIN domain to release the *Stachel*, while simultaneously perturbing ECL2 to allow displacement from the pocket. Once ECL2 moves, the released *Stachel* docks between the extracellular ends of the helices, adopting an active helical conformation and triggering canonical 7TMD rearrangements, including pronounced shifts in the extracellular end of TMH7 (Fig. 2c). This mechanism provides a “double-gating” logic at least for the cleavable GPR126: both *Stachel* release and ECL2 displacement are required for full receptor activation.

Differences in activation by antibody versus shaking suggest that the magnitude or type of external force determines ECL2 displacement and *Stachel* exposure. Notably, shaking produces ~ 10-fold higher activation than HA antibody, consistent with reports that mechanical stress partially unfolds the GAIN domain prior to dissociation [46].

Several open questions remain, including why specific ECL2 mutations differ in their functional effects between CTF and FL receptors (e.g., C902S, C985S) and the structural consequences of disulfide formation (absent in GPR126-$CTF_{ECL2\text{-}in}$ vs. present in GPR126-$CTF_{\textit{Stachel}\text{-}in}$). These differences highlight substantial remodeling at the extracellular interface upon activation and *Stachel* engagement, and suggest potential contributions from other ECLs, the NTF, or accessory proteins in modulating receptor activity.

Concluding remarks

Our data establish GPR126 ECL2 as a critical intramolecular regulator that gates access of the *Stachel* to the 7TMD. Unlike other GPCRs in which ECL2 can act as an agonist, here ECL2 restrains the true agonist, the *Stachel* core. The two cryo-EM structures (GPR126-$CTF_{ECL2\text{-}in}$ vs. GPR126-$CTF_{\textit{Stachel}\text{-}in}$), combined with mutational analysis, illuminate how GPR126 may toggle between inactive and active states, advancing our understanding of aGPCR activation and highlighting the broader principle that extracellular loops can control access of internal agonists in other GPCR families, with implications for mechanistic understanding and drug design.

Declarations

COMPETING INTERESTS

The authors declare no competing interests.

AUTHOR CONTRIBUTIONS

M.S. and A.H.A. established and performed the ADGRG6/GPR126 cell culture production and purification, with experimental input from M.G., D.S., A.K. and further advice from P.S.; M.S., M.G., D.S. and A.K. performed the Gs protein and antibody/Nb35 production. M.S. established and performed the GPR126-CTF–Gs–Nb35 complexation; M.S., A.H.A, L.K. and A.K. cloned all ADGRG6/GPR126 constructs; F.W., T.H., T.Sp. and M.S. performed the initial negative-stain and cryo-EM screening of the sample grids; F.W., T.H., T.Sp. and M.S prepared cryo-EM grids and collected images, F.W. reconstructed the final map and supervised the cryo-EM procedure with input of T.H., J.L. and C.M.T.S.; F.W. performed the cryo-EM data analysis with advice and input M.S., T.H., J.K., C.M.T.S and P.S.; F.W. built and refined the cryo-EM models with contributions from A.S. and P.S.; L.K. established and performed all signaling assays with input and advice of I.L.; G.K., M.S., L.K., T.S., I.L. and P.S. selected the ECL2 and other variants and interpreted the signaling data; G.K. performed the sequence analysis with support of T.S.; M.S., F.W., G.K. and P.S. analyzed the structures; F.W., M.S., G.K., L.K., I.L. and P.S. prepared the figures; G.K., T.S. and I.L. and P.S. wrote the manuscript with contributions of all co-authors. C.M.T.S., T.S., I.L. and P.S. initiated, supervised and funded the project; P.S. supervised the overall project. All authors edited and revised the manuscript.

ACKNOWLEDGMENTS

We thank Christine Gotthold for expert technical assistance. We thank Jörg Bürger for his help with cryo-EM sample preparation and acquisition. We acknowledge access to the Core Facility BioSupraMol at Freie Universität Berlin and to the Core Facility for cryo-Electron Microscopy (CFcryoEM) at Charité - Universitätsmedizin Berlin (both supported by the German Research Foundation (Deutsche Forschungsgemeinschaft, DFG) as well to the Technology Platform for cryo-Electron Microscopy at Max Delbrück Center for Moleculare Medicin in the Helmholtz Association (MDC).

This work was supported by the DFG through SFB1423, Project-ID 421152132, subprojects A01/Z03 (to P.S.), A05 (to T.S., C.M.T.S. and P.S.), B05 (to I.L.), C04 (to T.S.); through Germany´s Excellence Strategy – EXC 2008–390540038 – UniSysCat (Research Unit E) (to G.K. and P.S.); by the Minerva fellowship programme (funded by the German Federal Ministry for Education and Research) (to A.H.A.), by the European Union's Horizon 2020 research and innovation programme under the Marie Skłodowska-Curie grant agreement No 956314 [ALLODD] (to P.S.), by the Stiftung Charité fellow programme (to P.S.) and by the COST (European Cooperation in Science and Technology) Action CA18240 (Adher´nRise).

DATA AVAILABILITY

Structure model and EM maps for the GPR126-CTF$_{ECL2-in}$ was deposited to the Protein Data Bank with the accession code PDB-ID 34HS, EMD-59856 and the EM Data Bank with accession code EMD-59856.

MATERIAL AND METHODS

Structure Determination

Construct Design and Cloning

The human GPR126 (UniProtKB/Swiss-Prot: Q86SQ4) construct was engineered to enhance expression and facilitate purification. We generated a construct comprising amino acid residues 814–1222, which includes the *Stachel* sequence. An N-terminal hemagglutinin signal sequence was fused to a FLAG-tag epitope (DYKDDDK), and strategic insertions, deletions, and point mutations (detailed in Extended data Table 2) were introduced. At the C terminus, enhanced green fluorescent protein (eGFP) was appended, followed by polyhistidine (His-) and rho-1D4 tags; these tags are removable by HRV-3C protease cleavage. The final construct was subcloned into the pOET3 vector (pOET3_GPR126–eGFP). The heterotrimeric G-protein components were prepared as follows. The bovine Gα_s-short subunit (UniProtKB: P04896-2) was cloned into the pFastbac vector (construct pFastbac_Gas) as previously described [47]. The rat Gβ1 (UniProtKB: P54311) and bovine Gγ2 (UniProtKB: P63212) were cloned into the pFastbacDual vector (construct pFastbacDual_Gβ/Gγ) [48].

Baculovirus Production

Recombinant baculovirus for GPR126–eGFP was generated by co-transfecting Spodoptera frugiperda *Sf*9 cells with pOET3_GPR126–eGFP and linearized BAC10:1629KO [49] using Trans-IT Insect (Mirus Bio). *Sf*9 cells were cultured in Lonza *Sf*9 medium at 28 °C for 72 h to produce a potent P2 virus. Baculoviruses for Gαs, Gβ, and Gγ subunits were produced using the Bac-to-Bac™ system (Thermo Fisher Scientific). *Sf*9 cells were cultured in SF900 II serum-free medium (Invitrogen) at 28 °C for 72 h to generate potent P2 viruses.

In-Cell Complex Formation

*Sf*9 cells (1 L at 2 × 10⁶ cells/mL) were co-infected with P2 viruses for GPR126–eGFP, Gαs, and Gβ/Gγ at an empirically optimized volume ratio of 100:100:150 (10 mL: 10 mL: 5 mL, respectively). Cells were incubated at 27 °C and harvested by centrifugation 48 h post-infection. Cell pellets were stored at −20 °C until further use.

Nanobody 35 Expression and Purification

The single-domain antibody Nanobody-35 (Nb35) was expressed in *Escherichia coli* strain WK6. Following expression, Nb35 was extracted and purified using immobilized metal affinity chromatography (Ni-NTA) according to established protocols [50].

Complex Purification

*Sf*9 cell pellets containing GPR126–eGFP, Gα_s, and Gβ1Gγ2 from a 1 L culture were resuspended in Buffer A (20 mM HEPES, pH 7.5; 50 mM NaCl; 2 mM $MgCl_2$; 10% glycerol; 1 mM $CaCl_2$; 25 U/mL apyrase [New England Biolabs]; and one tablet cOmplete™ Protease Inhibitor Cocktail [Roche]). Seven milligrams of Nb35 were added, and the mixture was incubated for 2 h at 4 °C. Detergent solubilization was initiated by adding lauryl maltose neopentyl glycol (LMNG) and cholesteryl hemisuccinate (CHS; Anatrace, Inc.) to final concentrations of 0.5% and 0.05%, respectively. The suspension was gently mixed by repeated pipetting for 2 h at 4 °C. Following solubilization, the sample was ultracentrifuged at 30,000 rpm for 30 min at 4 °C. The resulting clear supernatant was diluted 1:1 with Buffer B (20 mM HEPES, pH 7.5; 50 mM NaCl; 2 mM $MgCl_2$; 1 mM $CaCl_2$) and loaded via peristaltic pump in a cold room onto a polypropylene column containing 1 mL HighSpec Rho1D4 Agarose (Cube Biotech). The column was washed with 50 mL of Buffer C (20 mM HEPES, pH 7.5; 50 mM NaCl; 2 mM $MgCl_2$; 1 mM $CaCl_2$; 0.05% LMNG; 0.005% CHS). Elution was performed by incubating the column overnight at 4 °C with Buffer E, which was identical to Buffer C except that it contained 200 µM rho1D4 peptide (TETSQVAPA) and 1 mg HRV-3C protease (in-house purified) [51,52] After elution, the complex was concentrated using a Vivaspin 500 concentrator (100 kDa cutoff) and further purified by size exclusion chromatography on a Superdex 200 Increase 5/150 GL column (Sigma-Aldrich) equilibrated with Buffer E. Fractions containing the receptor complex were pooled and concentrated to 5 mg/mL, then directly vitrified for cryo-EM analysis.

Cryo-EM Sample Preparation and Image Acquisition

Vitrification of GPR126-CTF–Gs–Nb35 complex was conducted immediately after sample preparation at a concentration of 1.0 mg/mL. 3.8 µL of the sample was applied to glow-discharged holey carbon grids (QuantiFoil R1.2/1.3 300 AU mesh, Quantifoil Micro Tools GmbH), blotted for 4 s and plunge-frozen in liquid ethane using an FEI Vitrobot Mark IV (Thermo Fisher Scientific) set to 10 °C and 100 % humidity.

Images were acquired using a FEI Titan Krios G3i microscope (Thermo Fisher Scientific) operated at 300 kV equipped with a FEI Falcon 3EC detector (Thermo Fisher Scientific) running in counting mode at a nominal magnification of 96,000×, giving a calibrated pixel size of 0.824 Å/px. Movies were recorded for 40.77 s accumulating a total electron dose of 43 e−/Å2 fractionated into 33 frames. EPU 2.8 was utilized for automated data acquisition with AFIS enabled using a nominal defocus between −1 and −2 µm. A total of 5,929 micrographs were collected. These were used for further image processing. Further details are given in Extended data Table 3.

Cryo-EM Image Processing

The entire data analysis was conducted within the cryoSPARC v4.60 [53] framework (Extened data Figs. 3–4). Image analysis started with movie alignment and dose-weighting using “Patch motion correction” followed by “Patch CTF estimation”. Initial particle picking was done with “Blob picker” using a particle diameter of 180 Å. Particle images were extracted with a box size of 280 px, Fourier-cropped to 70 px (3.296 Å/px). After reference-free 2D classification, selected class averages were used for ab initio

reconstruction followed by hetero refinement resulting in an initial structure of the complex. Templates created from that volume were used for template-based particle picking with a 170 Å particle mask. A total of 3,431,742 particle images were subjected to two cycles of 2D classification to clean the dataset. Ab initio reconstruction of particle images belonging to shiny classes was applied to generate a reference model for 3D classification. Shiny particles of this initial structure evaluation were used to train a model-picking-algorithm in TOPAZ [54].

Re-picking using this trained model resulted in 1,860,602 particles. These were extracted with a box size of 300 px, Fourier-cropped to 100 px (2.472 Å/px). They underwent two independent rounds of 2D-classification followed by heterogenous refinement as described above. 165,942 complex particles from these independent sortings were combined and re-extracted unbinned (300 px, 0.824 Å/px). A further 2D classification removed non-shiny particles reducing the dataset to 146,999 particles. After NU refinement applying CTF correction this resulted in a consensus structure with global resolution of 3.27 Å. These particles were used for 3D-variability analysis in principal component analysis mode with a focus mask on the G-protein region at a filter resolution of 4 Å. The results were clustered into two structures (66,197 and 69,386 particles respectively) that showed different orientation of transmembrane helices, ECL2 and *Stachel*. Particles that did not show complex structures (11,416 particles) were discarded. Further 3D variability analysis showed variability for one state which sorted again in the same way. Of the resulting two structures one showed the same conformation as the one sorted before and was combined. This resulted in two different structures with 101,791 particles belonging to a *Stachel* unbound state (GPR126-CTF$_{ECL2\text{-}in}$) and 33,792 particles to one that showed *Stachel*-density in the binding pocket (GPR126-CTF$_{\textit{Stachel}\text{-}in}$), respectively. A final NU refinement for the GPR126-CTF$_{\textit{Stachel}\text{-}in$–Gs–Nb35 complex resulted in a reconstruction of 3.8 Å global resolution, while the GPR126-CTF$_{ECL2\text{-}in}$–Gs–Nb35 complex was refined to 3.38 Å global resolution.

Model Building and Refinement

A homology model for GPR126 complex was derived from GPR64 structure (PDB-ID: 7wuq [55]) together with the G_sαβγ–Nb35 complex of the NDP-α-MSH–MC4R–Gs complex (PDB-ID: 7piv [56]) and used as initial model. The complex was built and adjusted manually in the program COOT v0.9.6.4 [57]. using an auto-sharpened map (using CryoSPARC) and additionally a low-pass-filtered map to 4 Å for more mobile regions as ECL2. After every round of manual refinement and for the final round, real-space refinement was performed with the program phenix.refine from PHENIX v.1.19 [58] using geometric restraints, a global minimization protocol and B-factor refinement. The model was validated using Molprobity and OneDep [59] of the Protein Data Bank (Extended Data Table 3).

The final structure model of the GPR126-CTF$_{ECL2\text{-}in}$–Gs–Nb35 complex comprises the following residues: GPR126-CTF 830-1100 (excluding several residues in ICL3: 1025-1031), Gα$_s$ protein: 14-47, 193-236, 248-280, 293-351, 355-380; Gβ protein: 4-340; Gγ protein: 9-63, Nb35: 1-128. Residues 312-318 of Gα$_s$ were modeled as alanine due to poorly resolved side chain density.

The final structure model of the GPR126-CTF$_{Stachel\text{-}in}$–Gs–Nb35 complex comprises the following residues: GPR126-CTF 814-825 and 831-1100 (excluding several residues in ICL2: 971-982 and ICL3: 1026-1032), Gα_s protein: 14-47, 193-236, 248-280, 293-351, 355-380; Gβ protein: 4-340; Gγ protein: 9-63, Nb35: 1-128. Residues 312-318 of Gα_s were modeled as alanine due to poorly resolved side chain density.

Potential hydrogen bonds and van der Waals contacts were analyzed using HBPLUS and LigPlot+ v2.2.9 [60]. All molecular graphics representations in this work were created using the PyMOL Molecular Graphics System, Version 2.5.5 and 3.1.3, Schrödinger, LLC., UCSF Chimera v.1.16 [61] and UCSF ChimeraX v1.7 [61,62].

Molecular Biology

If not stated otherwise, all standard substances were ordered from Sigma Aldrich (Taufkirchen, Germany), Merck (Darmstadt, Germany), and C. Roth GmbH (Karlsruhe, Germany). Cell culture material was obtained from Thermo Fisher Scientific (Schwerte, Germany), and primers were obtained from Microsynth Seqlab GmbH (Göttingen, Germany).

Constructs and Cloning

The CTF and full-length constructs of human GPR126 in pcDps carry an N-terminal HA-tag and a C-terminal FLAG-tag previously described [47]. All point mutations and deletions were cloned by using QuikChange site directed mutagenesis. Briefly, plasmid DNA was amplified by PCR and accordingly digested with *Dpn*I restriction enzyme (New England Biolabs, MA, USA) for 1 h at 37 °C. Afterwards, *E. coli* cells were transformed by heat shock.

Surface Expression

To analyze the surface expression, a cellular enzyme-linked immunosorbent assay (ELISA) was used [63]. The COS-7 or HEK293T cells were split into a 48-well plate ($3x10^4$ COS-7 cells per well, $5x10^4$ HEK293T cells per well) and cultivated in Dulbecco's minimum essential medium (DMEM) supplemented with 10 % fetal bovine serum (FBS), 100 units/mL penicillin, and 100 µg/mL streptomycin at 37 °C and 5 % CO_2 in a humidified atmosphere. The transfection was performed with Lipofectamine 2000 (Thermo Fisher Scientific) according to manufactures protocol using 500 ng/well up to 1000 ng/well (titration experiment). After 48 h, the cells were fixed with 4 % formaldehyde, washed with DPBS and blocked with DMEM supplemented with 10 % FBS. Afterwards, the fixed cells were incubated with Anti HA POD conjugated antibody followed by *o*-phenylendiamine treatment. The optical density was measured at a wavelength of 492 nm and 620 nm with Infinite 200 Pro, Tecan Austria GmbH.

Whole Cell Expression

To analyze the whole cell expression, a sandwich enzyme-linked immunosorbent assay (ELISA) was used[63]. The COS-7 or HEK293T cells were split into a 6-well plate ($3x10^5$ per well) and cultivated in DMEM supplemented with 10 % FBS, 100 units/mL penicillin, and 100 µg/mL streptomycin at 37 °C and 5 % CO_2 in a humidified atmosphere. The transfection was performed with Lipofectamine 2000 (Thermo Fisher Scientific) according to manufactures protocol using 1000 ng DNA/well. After 48 h, the cells were detached with DPBS, solubilized overnight and a 96-well plate was coated with M2 FLAG antibody (F3165, Sigma-Aldrich).

Afterwards, the 96-well plate was washed with PBS-T, blocked with DMEM supplemented with 10% FBS, incubated with the solubilized samples, and incubated with anti-HA POD-conjugated antibody followed by *o*-phenylendiamine treatment. The optical density was measured at a wavelength of 492 nm and 620 nm with Infinite 200 Pro, Tecan Austria GmbH.

Peptide Stimulation Assay

The receptor constructs were heterologous expressed in HEK293T cells cultivated in DMEM supplemented with 10 % FBS, 100 units/mL penicillin, and 100 µg/mL streptomycin at 37 °C and 5 % CO_2 in a humidified atmosphere. The cells were distributed into a 96-well plate ($1.5x10^4$ cells per well). The transfection was performed with Lipofectamine 2000 (Thermo Fisher Scientific) according to manufactures protocol using 50 ng up to 100 ng DNA/well (96-well plate) depending on the surface expression.

After 48 h, the basal activity assay was performed by adding 3-isobutylmethyl-xanthine (1 mM)-(IBMX)-containing medium and incubated for 30 min at 37 °C, 5 % CO_2 humidified atmosphere. For the peptide stimulation, the peptide corresponding to the *Stachel* sequence of GPR126 (p126) was solubilized in Tris pH 8.0 to the stock concentration of 10 mM. The peptides 17AA (YGKESYGKEKGDEFCWI) and 12AA (KESYGKEKGDEF) corresponding to the ECL2 sequence of GPR126 were solubilized in Tris pH 8.0 with 10 % DMSO to the stock concentration of 10 mM.

The p126 peptide was diluted to the final concentration (500 µM) in IBMX-containing medium. The cells incubated with final peptide concentration for 30 min at 37 °C, 5 % CO_2 humidified atmosphere. After stimulation, the cells were lysed in LI buffer (PerkinElmer, Rodgau, Germany) and frozen at -20 °C until measurement.

For the combined stimulation of WT GPR126-FL and GPR126-CTF with peptides corresponding to the ECL2 sequence of GPR126, the peptides 17AA and 12AA were diluted to the final concentration (1 µM, 10 µM, 100 µM, 1 mM) in IBMX-containing medium. The stimulation was performed in absence or presence of 100 µM p126 peptide for 30 min at 37 °C, 5 % CO_2 humidified atmosphere. After stimulation, the cells were lysed in LI buffer (PerkinElmer, Rodgau, Germany) and frozen at -20 °C until measurement. To measure cAMP concentration, the AlphaScreen cAMP assay kit (PerkinElmer) was used according to

the manufacturer's protocol. The accumulation was measured in a 384-well white OptiPlate microplate (PerkinElmer) by using the EnVision Multilabel Reader (PerkinElmer).

HA Antibody Activation

The full-length GPR126-FL constructs were heterologous expressed in COS-7 cells cultivated in DMEM supplemented with 10 % FBS, 100 units/mL penicillin, and 100 µg/mL streptomycin at 37 °C and 5 % CO_2 in a humidified atmosphere. The cells were distributed into a 48-well plate ($3x10^4$ cells per well).

The transfection was performed with Lipofectamine 2000 (Thermo Fisher Scientific) according to manufactures protocol using 500 ng up to 1000 ng DNA/per well (48-well plate) depending on the surface expression.

The stimulation was performed by diluting the anti–HA antibody (H3663, stock concentration 1 mg/mL, Sigma-Aldrich) 1:1000 in IBMX-containing medium and incubated for 30 min at 37 °C, 5 % CO_2 humidified atmosphere [39].

Afterwards, the cells were lysed in LI buffer and stored at -20 °C until measurement. The cAMP concentration was measured via the AlphaScreen cAMP assay kit (PerkinElmer).

Mechano-Activation Assay

The GPR126-FL constructs were heterologous expressed in HEK293T cells cultivated in DMEM supplemented with 10 % FBS, 100 units/mL penicillin, and 100 µg/mL streptomycin at 37 °C and 5 % CO_2 in a humidified atmosphere. The cells were distributed into a 12-well plate ($2x10^5$ cells per well). The transfection was performed with Lipofectamine 2000 (Thermo Fisher Scientific) according to manufactures protocol using 1000 ng DNA/per well (12-well plate).

For the mechano-activation assay, the cells were detached with DPBS, centrifuged and suspended in IBMX-containing medium. Then, the cell suspension was incubated under static or shaking (200 rpm) conditions for 30 min, 37 °C. Afterwards, the cells were lysed in LI buffer and stored at -20 °C until measurement. The cAMP concentration was measured via the AlphaScreen cAMP assay kit (PerkinElmer).

Sequence Alignment and Figure Visualization

Structural representations were generated using PyMol (Molecular Graphics System Version 2.5.5, Schrödinger, LLC, New York, NY). The sequence alignment was generated by using ClustalW [64] followed by manual corrections and visualization with the software package BioEdit [65].

References

1. Wittlake A, Promel S, Schoneberg T (2021) The Evolutionary History of Vertebrate Adhesion GPCRs and Its Implication on Their Classification. Int J Mol Sci 22. https://doi.org/10.3390/ijms222111803
2. Hamann J et al (2015) International Union of Basic and Clinical Pharmacology. XCIV. Adhesion G protein-coupled receptors. Pharmacol Rev 67:338–367. https://doi.org/10.1124/pr.114.009647
3. Langenhan T et al (2026) Adhesion G protein-coupled receptors. Pharmacol Rev 78:100116. https://doi.org/10.1016/j.pharmr.2026.100116
4. Petersen SC et al (2015) The adhesion GPCR GPR126 has distinct, domain-dependent functions in Schwann cell development mediated by interaction with laminin-211. Neuron 85:755–769. https://doi.org/10.1016/j.neuron.2014.12.057
5. Ping YQ et al (2022) Structural basis for the tethered peptide activation of adhesion GPCRs. Nature 604:763–770. https://doi.org/10.1038/s41586-022-04619-y
6. Wilde C et al (2016) The constitutive activity of the adhesion GPCR GPR114/ADGRG5 is mediated by its tethered agonist. FASEB J 30:666–673. https://doi.org/10.1096/fj.15-276220
7. Zhong BL et al (2023) Piconewton Forces Mediate GAIN Domain Dissociation of the Latrophilin-3 Adhesion GPCR. Nano Lett 23:9187–9194. https://doi.org/10.1021/acs.nanolett.3c03171
8. Lala T, Hall RA, Adhesion (2022) G protein-coupled receptors: structure, signaling, physiology, and pathophysiology. Physiol Rev 102:1587–1624. https://doi.org/10.1152/physrev.00027.2021
9. Schoneberg T, Liebscher I (2021) Mutations in G Protein-Coupled Receptors: Mechanisms, Pathophysiology and Potential Therapeutic Approaches. Pharmacol Rev 73:89–119. https://doi.org/10.1124/pharmrev.120.000011
10. Arac D et al (2012) A novel evolutionarily conserved domain of cell-adhesion GPCRs mediates autoproteolysis. EMBO J 31:1364–1378. https://doi.org/10.1038/emboj.2012.26
11. Lin HH et al (2004) Autocatalytic cleavage of the EMR2 receptor occurs at a conserved G protein-coupled receptor proteolytic site motif. J Biol Chem 279:31823–31832. https://doi.org/10.1074/jbc.M402974200
12. Liebscher I, Schoneberg T, Tethered Agonism (2016) A Common Activation Mechanism of Adhesion GPCRs. Handb Exp Pharmacol 234:111–125. https://doi.org/10.1007/978-3-319-41523-9_6
13. Kleinau G et al (2023) Intramolecular activity regulation of adhesion GPCRs in light of recent structural and evolutionary information. Pharmacol Res 197:106971. https://doi.org/10.1016/j.phrs.2023.106971
14. Liebscher I et al (2014) A tethered agonist within the ectodomain activates the adhesion G protein-coupled receptors GPR126 and GPR133. Cell Rep 9:2018–2026. https://doi.org/10.1016/j.celrep.2014.11.036
15. Shriver T et al (2026) The isolated Stachel peptide of the adhesion G protein-coupled receptor GPR126 is intrinsically disordered. *bioRxiv* https://doi.org/10.64898/2026.01.16.700034
16. Seufert F, Chung YK, Hildebrand PW, Langenhan T (2023) 7TM domain structures of adhesion GPCRs: what's new and what's missing? Trends Biochem Sci 48:726–739.

https://doi.org/10.1016/j.tibs.2023.05.007

17. Leon K et al (2020) Structural basis for adhesion G protein-coupled receptor Gpr126 function. Nat Commun 11:194. https://doi.org/10.1038/s41467-019-14040-1
18. Qiu N et al (2026) Extra-helical allosteric binding site of apomorphine in ADGRG6. Cell Discov 12:9. https://doi.org/10.1038/s41421-025-00866-1
19. Li Q et al (2024) Structure, ligands, and roles of GPR126/ADGRG6 in the development and diseases. Genes Dis 11:294–305. https://doi.org/10.1016/j.gendis.2023.02.016
20. Suchy T et al (2020) The repertoire of Adhesion G protein-coupled receptors in adipocytes and their functional relevance. Int J Obes (Lond) 44:2124–2136. https://doi.org/10.1038/s41366-020-0570-2
21. Musa G et al (2019) Gpr126 (Adgrg6) is expressed in cell types known to be exposed to mechanical stimuli. Ann N Y Acad Sci 1456:96–108. https://doi.org/10.1111/nyas.14135
22. Paavola KJ, Sidik H, Zuchero JB, Eckart M, Talbot WS (2014) Type IV collagen is an activating ligand for the adhesion G protein-coupled receptor GPR126. Sci Signal 7:ra76. https://doi.org/10.1126/scisignal.2005347
23. Wilde C et al (2023) Collagen VI Is a Gi-Biased Ligand of the Adhesion GPCR GPR126/ADGRG6. *Cells* 12 https://doi.org/10.3390/cells12111551
24. Barros-Alvarez X et al (2022) The tethered peptide activation mechanism of adhesion GPCRs. Nature 604:757–762. https://doi.org/10.1038/s41586-022-04575-7
25. Lin H et al (2022) Structures of the ADGRG2-G(s) complex in apo and ligand-bound forms. Nat Chem Biol 18:1196–1203. https://doi.org/10.1038/s41589-022-01084-6
26. Ping YQ et al (2021) Structures of the glucocorticoid-bound adhesion receptor GPR97-G(o) complex. Nature 589:620–626. https://doi.org/10.1038/s41586-020-03083-w
27. Yang Z et al (2025) Identification, structure, and agonist design of an androgen membrane receptor. *Cell* 188, 1589–1604 e1524 https://doi.org/10.1016/j.cell.2025.01.006
28. Zhu X et al (2022) Structural basis of adhesion GPCR GPR110 activation by stalk peptide and G-proteins coupling. Nat Commun 13:5513. https://doi.org/10.1038/s41467-022-33173-4
29. Cullum SA et al (2024) Mechano-sensitivity of beta2-adrenoceptors enhances constitutive activation of cAMP generation that is inhibited by inverse agonists. Commun Biol 7:417. https://doi.org/10.1038/s42003-024-06128-2
30. Seibt BF et al (2013) The second extracellular loop of GPCRs determines subtype-selectivity and controls efficacy as evidenced by loop exchange study at A2 adenosine receptors. Biochem Pharmacol 85:1317–1329. https://doi.org/10.1016/j.bcp.2013.03.005
31. Unal H, Jagannathan R, Bhat MB, Karnik SS (2010) Ligand-specific conformation of extracellular loop-2 in the angiotensin II type 1 receptor. J Biol Chem 285:16341–16350. https://doi.org/10.1074/jbc.M109.094870
32. Asada H et al (2018) Crystal structure of the human angiotensin II type 2 receptor bound to an angiotensin II analog. Nat Struct Mol Biol 25:570–576. https://doi.org/10.1038/s41594-018-0079-8

33. Bokoch MP et al (2010) Ligand-specific regulation of the extracellular surface of a G-protein-coupled receptor. Nature 463:108–112. https://doi.org/10.1038/nature08650
34. Erlandson SC et al (2023) The relaxin receptor RXFP1 signals through a mechanism of autoinhibition. Nat Chem Biol 19:1013–1021. https://doi.org/10.1038/s41589-023-01321-6
35. Wong TS et al Cryo-EM structure of orphan G protein-coupled receptor GPR21. *MedComm (*(2020)) 4, e205 (2023).) 4, e205 (2023). https://doi.org/10.1002/mco2.205
36. Massotte D, Kieffer BL (2005) The second extracellular loop: a damper for G protein-coupled receptors? Nat Struct Mol Biol 12:287–288. https://doi.org/10.1038/nsmb0405-287
37. Qu X et al (2022) Structural basis of tethered agonism of the adhesion GPCRs ADGRD1 and ADGRF1. Nature 604:779–785. https://doi.org/10.1038/s41586-022-04580-w
38. Zhong P et al (2026) Molecular basis of antagonism of the dimeric human arginine vasopressin receptor 1A. Nat Commun 17:1622. https://doi.org/10.1038/s41467-026-68331-5
39. Mitgau J et al (2022) The N Terminus of Adhesion G Protein-Coupled Receptor GPR126/ADGRG6 as Allosteric Force Integrator. Front Cell Dev Biol 10:873278. https://doi.org/10.3389/fcell.2022.873278
40. Ye F et al (2022) Cryo-EM structure of G-protein-coupled receptor GPR17 in complex with inhibitory G protein. MedComm (2020) 3:e159. https://doi.org/10.1002/mco2.159
41. Lin X et al (2020) Structural basis of ligand recognition and self-activation of orphan GPR52. Nature 579:152–157. https://doi.org/10.1038/s41586-020-2019-0
42. Tsutsumi N et al (2021) Structural basis for the constitutive activity and immunomodulatory properties of the Epstein-Barr virus-encoded G protein-coupled receptor BILF1. *Immunity* 54, 1405–1416 e1407 https://doi.org/10.1016/j.immuni.2021.06.001
43. Liu A et al (2024) Structural insights into KSHV-GPCR constitutive activation and CXCL1 chemokine recognition. Proc Natl Acad Sci U S A 121:e2403217121. https://doi.org/10.1073/pnas.2403217121
44. Howard MK et al (2025) Molecular basis of proton sensing by G protein-coupled receptors. *Cell* 188, 671–687 e620 https://doi.org/10.1016/j.cell.2024.11.036
45. Xu J et al (2018) GPR68 Senses Flow and Is Essential for Vascular Physiology. *Cell* 173, 762–775 e716 https://doi.org/10.1016/j.cell.2018.03.076
46. Fu C et al (2023) Unveiling Mechanical Activation: GAIN Domain Unfolding and Dissociation in Adhesion GPCRs. Nano Lett 23:9179–9186. https://doi.org/10.1021/acs.nanolett.3c01163
47. Liang YL et al (2017) Phase-plate cryo-EM structure of a class B GPCR-G-protein complex. Nature 546:118–123. https://doi.org/10.1038/nature22327
48. Rasmussen SG et al (2011) Crystal structure of the beta2 adrenergic receptor-Gs protein complex. Nature 477:549–555. https://doi.org/10.1038/nature10361
49. Berger I, Fitzgerald DJ, Richmond TJ (2004) Baculovirus expression system for heterologous multiprotein complexes. Nat Biotechnol 22:1583–1587. https://doi.org/10.1038/nbt1036
50. Pardon E et al (2014) A general protocol for the generation of Nanobodies for structural biology. Nat Protoc 9:674–693. https://doi.org/10.1038/nprot.2014.039

51. Corin K et al (2011) Structure and function analyses of the purified GPCR human vomeronasal type 1 receptor 1. Sci Rep 1:172. https://doi.org/10.1038/srep00172
52. Oprian DD, Molday RS, Kaufman RJ, Khorana HG (1987) Expression of a synthetic bovine rhodopsin gene in monkey kidney cells. Proc Natl Acad Sci U S A 84:8874–8878. https://doi.org/10.1073/pnas.84.24.8874
53. Punjani A, Rubinstein JL, Fleet DJ, Brubaker MA (2017) cryoSPARC: algorithms for rapid unsupervised cryo-EM structure determination. Nat Methods 14:290–296. https://doi.org/10.1038/nmeth.4169
54. Bepler T et al (2019) Positive-unlabeled convolutional neural networks for particle picking in cryo-electron micrographs. Nat Methods 16:1153–1160. https://doi.org/10.1038/s41592-019-0575-8
55. Xiao P et al (2022) Tethered peptide activation mechanism of the adhesion GPCRs ADGRG2 and ADGRG4. Nature 604:771–778. https://doi.org/10.1038/s41586-022-04590-8
56. Heyder NA et al (2021) Structures of active melanocortin-4 receptor-Gs-protein complexes with NDP-alpha-MSH and setmelanotide. Cell Res 31:1176–1189. https://doi.org/10.1038/s41422-021-00569-8
57. Emsley P, Lohkamp B, Scott WG, Cowtan K (2010) Features and development of Coot. Acta Crystallogr D Biol Crystallogr 66:486–501. https://doi.org/10.1107/S0907444910007493
58. Liebschner D et al (2019) Macromolecular structure determination using X-rays, neutrons and electrons: recent developments in Phenix. Acta Crystallogr D Struct Biol 75:861–877. https://doi.org/10.1107/S2059798319011471
59. Young JY et al (2017) OneDep: Unified wwPDB System for Deposition, Biocuration, and Validation of Macromolecular Structures in the PDB Archive. Structure 25:536–545. https://doi.org/10.1016/j.str.2017.01.004
60. Laskowski RA, Swindells MB (2011) LigPlot+: multiple ligand-protein interaction diagrams for drug discovery. J Chem Inf Model 51:2778–2786. https://doi.org/10.1021/ci200227u
61. Pettersen EF et al (2004) UCSF Chimera–a visualization system for exploratory research and analysis. J Comput Chem 25:1605–1612. https://doi.org/10.1002/jcc.20084
62. Meng EC et al (2023) UCSF ChimeraX: Tools for structure building and analysis. Protein Sci 32:e4792. https://doi.org/10.1002/pro.4792
63. Schoneberg T, Yun J, Wenkert D, Wess J (1996) Functional rescue of mutant V2 vasopressin receptors causing nephrogenic diabetes insipidus by a co-expressed receptor polypeptide. EMBO J 15:1283–1291
64. Thompson JD, Higgins DG, Gibson TJ (1994) CLUSTAL W: improving the sensitivity of progressive multiple sequence alignment through sequence weighting, position-specific gap penalties and weight matrix choice. Nucleic Acids Res 22:4673–4680. https://doi.org/10.1093/nar/22.22.4673
65. Hall TA (1999) BioEdit: a user-friendly biological sequence alignment editor and analysis program for Windows 95/98/NT. *Nucleic Acids Symposium Series* 41, 95–98

Figures

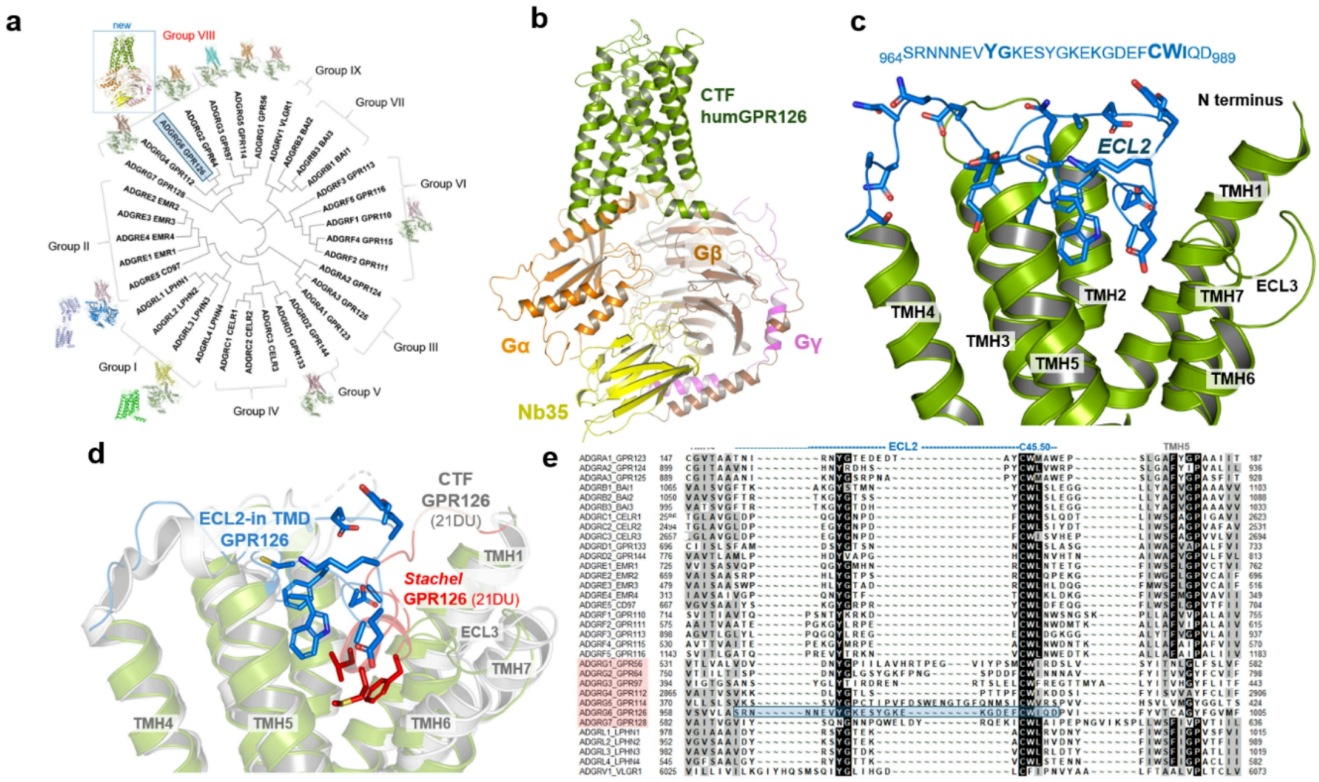

Figure 1

Cryo-EM structure of the GPR126$_{ECL2\text{-}in}$–CTF/G$_s$/Nb35 complex and ECL2 features. (**a**) Phylogenetic tree of human aGPCRs based on CTF sequences. Most available CTF structures correspond to group VIII receptors. (**b**) Cartoon of the human GPR126$_{ECL2\text{-}in}$-CTF–G$_s$–Nb35 complex showing ECL2 bound within the receptor core (*Stachel* not resolved). (**c**) Close-up of the 7TMD highlighting the *Stachel*-binding pocket occupied by ECL2 (blue). Side chains are shown as sticks. Conserved residues in the GPR126 ECL2 sequence are indicated in bold above. (**d**) Superposition of the GPR126$_{ECL2\text{-}in}$ structure with the previously reported GPR126-CTF–G$_s$ structure (PDB-ID: 21DU [18]). ECL2 (blue, sticks) partially occupies the canonical *Stachel*-binding site that accommodates the helical *Stachel* (red; 7TMD backbone in grey) in the published structure. (**e**) Sequence alignment of ECL2 from all 33 human aGPCRs (conserved residues in grey; group VIII in red; GPR126 ECL2 in blue). Structural length of ECL2 is indicated above, along with the reference position for the unified class B ECL2 numbering (C45.50) [13]. Key residues discussed in the text are annotated using this system to allow comparison across class B1 and B2 receptors.

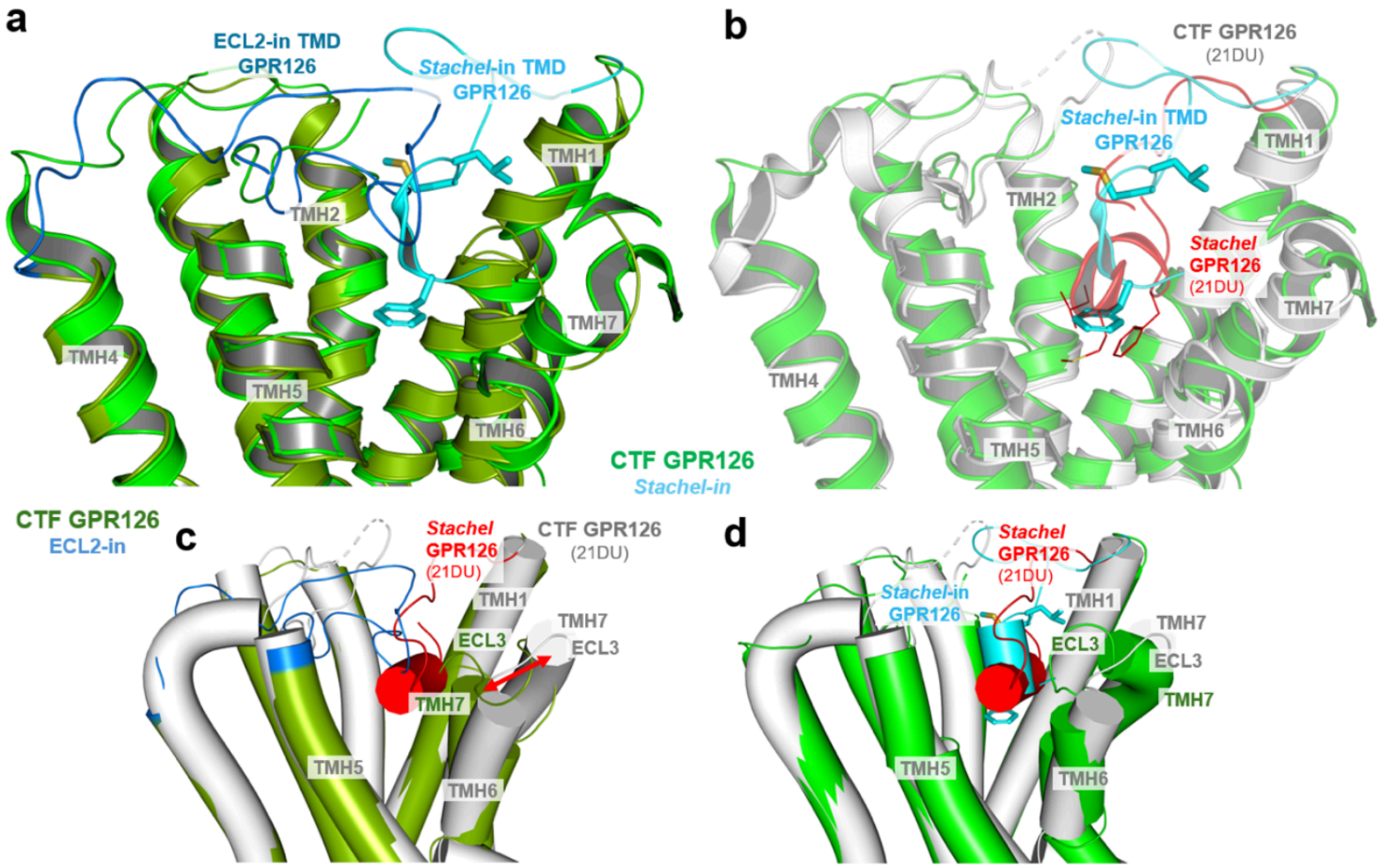

Figure 2

GPR126 with bound Stachel (GPR126$_{Stachel\text{-}in}$) and backbone comparison with the GPR126–*Stachel* structure. (**a**) Cryo-EM structure of GPR126$_{Stachel\text{-}in}$ in complex with G_s, resolved at 3.7 Å. The *Stachel* is bound within the 7TMD and adopts an unusual fold and orientation. (**b**) Comparison with the previously published GPR126–*Stachel* structure (PDB-ID: 21DU [18]) highlights differences in *Stachel* conformation and binding mode. (**c**) Superposition of GPR126$_{ECL2\text{-}in}$ with the published GPR126–*Stachel* structure (red) reveals specific differences in TMH7 and ECL3, which connects TMH6 and TMH7. (**d**) In the partially bound GPR126$_{Stachel\text{-}in}$ structure, TMH7 adopts a conformation similar to canonical *Stachel*-bound states, while ECL3 shows notable deviations.

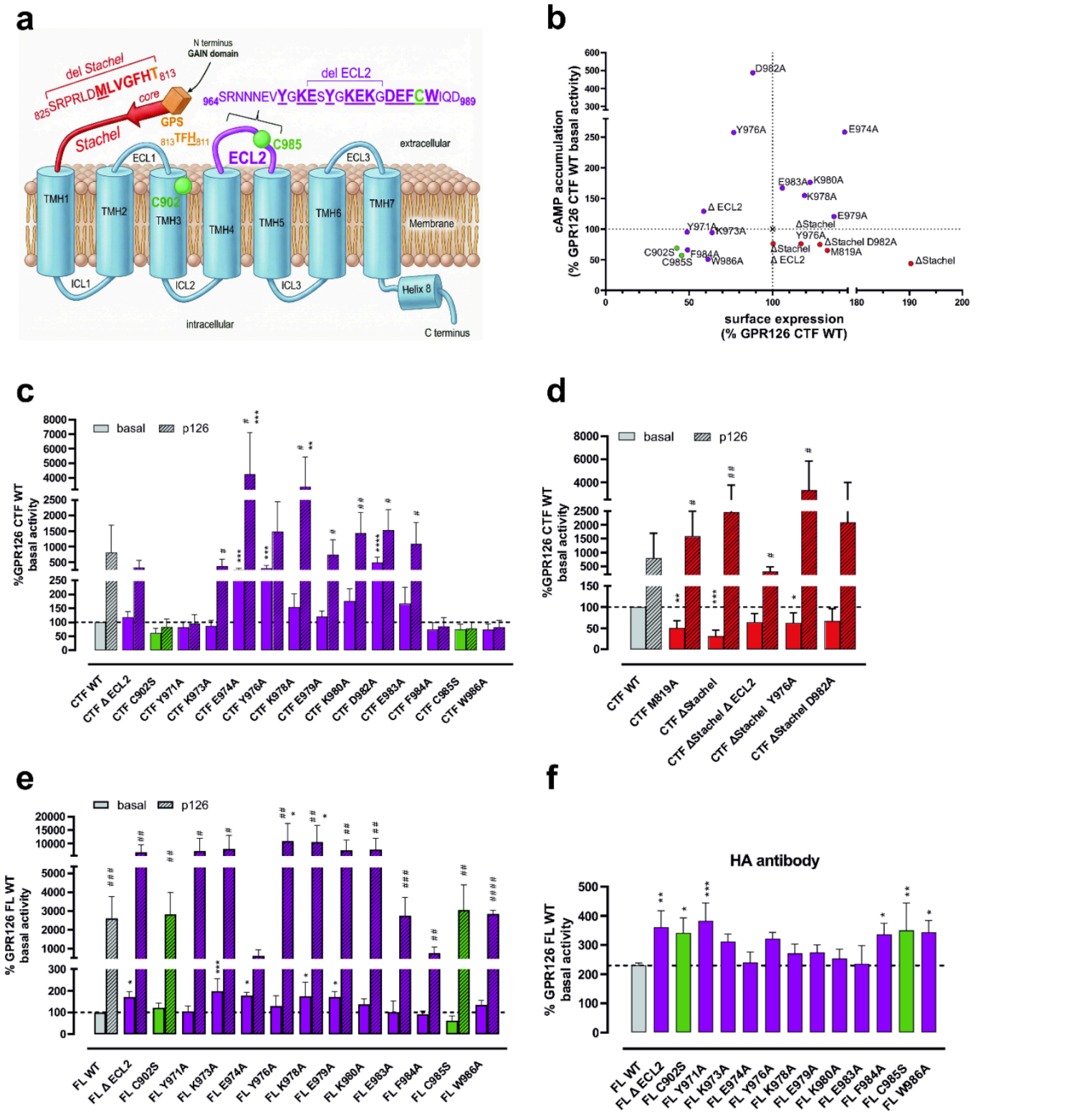

Figure 3

Functional characterization of GPR126-CTF and GPR126 full-length ECL2 variants. (**a**) Scheme of the GPR126 with indicated structural parts and sequences of the ECL2, *Stachel* core and GPS. Mutated positions are underlined and enlarged. (**b**) Cell surface expression and basal cAMP accumulation of GPR126-CTF ECL2 mutants. (**c**) Basal and p126-induced activity of GPR126-CTF ECL2 mutants after correction for comparable surface expression. (**d**) Basal and p126-induced cAMP accumulation in WT

and ECL2 GPR126-CTF *Stachel* mutants. (**e**) Basal and p126-induced cAMP accumulation in WT and ECL2 GPR126-FL variants. (**f**) Accumulated cAMP levels in ECL2 GPR126-FL variants upon activation with HA antibody. Data are presented as mean ± SD, n = 4–5 (each in triplicate). Statistical analysis was performed using one-way ANOVA (*p < 0.05; **p < 0.01; ***p < 0.001, mutant vs. WT) and paired t-test (#p < 0.05; ##p < 0.01; ###p < 0.001, basal vs. stimulated for each construct).

Supplementary Files

This is a list of supplementary files associated with this preprint. Click to download.

- Validationreports.zip
- nrreportingsummaryGPR126final2.pdf
- dataaccessdetails.docx
- ExtendedMaterialWiechertetalNC2026New.pdf